EPJ Web of Conferences **193**, 01001 (2018) https://doi.org/10.1051/epjconf/201819301001
FISSION 2017

Shells, Anti-Shells and Modes in nuclear Fission

Friedrich Gönnenwein

Universität Tübingen, 72076 Tübingen, Germany

Abstract. Fission phenomena are surveyed where fragment properties are catching the eye. Beyond the Liquid Drop the relevant properties of fragments are shell effects and nuclear pairing. Shell effects influence on mass, charge, stability and deformability of fragments. Most often only the stabilizing effects of shells are discussed and the equally frequent destabilizing effects are not mentioned. For the present purpose the terms shells and anti-shells are used in case of stabilizing and destabilizing effects, respectively. Fragment shells and anti-shells lead to fission modes with characteristic properties. A special issue is where in the course of fission these modes assume their characteristic features. Surprisingly fragment angular distributions in above- and sub-barrier fission help elucidating this question. The discussion is focussed on fission in the standard actinides.

1 Liquid Drop Model, shells and anti-shells

The Liquid Drop Model (LDM) of nuclei has since the discovery of fission been the backbone of our understanding of the fission process. A major drawback of the model is however the prediction of symmetric mass distribution of fission fragments. Asymmetric fission observed in the standard actinides remained a puzzle until the advent of the shell model.

For convenience, the mass M(A,Z) in the LDM of a nucleus with mass and charge numbers A and Z, respectively, is recalled in eq. (1) as the sum of volume, surface, Coulomb, symmetry and pairing terms:

$$M(A,Z) = a_V A + a_S A^{2/3} + a_C Z^2/A^{1/3} + a_I (N-Z)^2/A - \delta(A). \quad (1)$$

The macroscopic LDM describes with a few parameters the average mass of nuclei across the chart of nuclides. However, the microscopic nuclear structure requires corrections. A first comprehensive survey of these corrections was proposed in 1966 by W. Myers and W. Swiatecki [1]. The shell correction δW is defined as the difference between the experimental mass M_{exp} taken from mass tables and the LDM mass M_{LDM}:

$$\delta W = M_{exp} - M_{LDM}. \quad (2)$$

The shell corrections were calculated separately for neutron and proton numbers N and Z. An example is provided in Fig. 1 for a range of neutron numbers. In the figure the shell correction is seen to oscillate between $\delta W > 0$ and $\delta W < 0$. The familiar case is $\delta W < 0$.

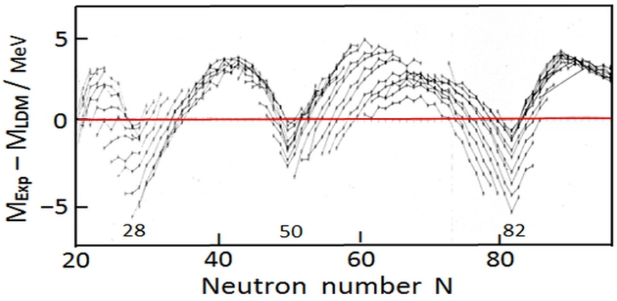

Fig. 1: Shell correction for neutron numbers N = 20 to N = 95. Adapted from [1].

Relative to the LDM the nuclear mass is here smaller indicating that these nuclei are more tightly bound. As seen in Fig .1 the minima correspond to the famous magic neutron numbers N = 28, 50 and 82 for stable nuclei. But it is evident that for more nuclei the correction is δW > 0, with nuclei less tightly bound than in the LDM. For convenience it is proposed to call nuclei with δW < 0 shell nuclei, and nuclei with δW < 0 anti-shell nuclei.

To assess shell or anti-shell corrections for fission fragments, the N and Z content of fragments has to be taken into account. This has been done for several common reactions in the actinides by A. Ruben and H. Märten [2]. The result is plotted in Fig. 2. There is a marked

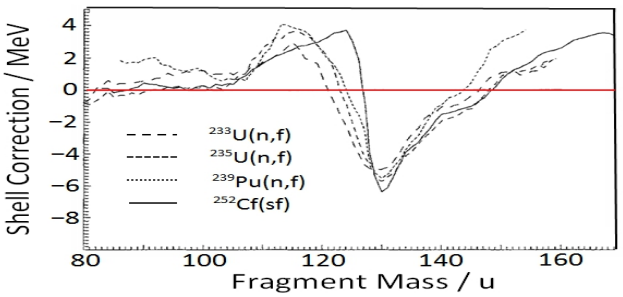

Fig. 2: Shell correction δW *vs* fragment mass for several fission reactions. Adapted from [2].

shell effect for masses around A = 130 u and pronounced anti-shell effects for masses around A = 120 u and masses larger than A = 145 u.

Besides stability shell and anti-shell nuclei differ in their stiffness properties. Stiffness describes the resistance of a nucleus against deformation. For spheroids the deformation E_{def} is parameterized by

$$E_{def} = \alpha(D - R_0)^2 \quad (3)$$

with D the major semi-axis of the spheroid, R_0 the radius of the spherical nucleus with same volume and α the stiffness parameter. The stiffness has been measured in Coulex experiments probing vibrational resonances in e-e nuclei. The stiffness data α/α_{LDM} of these nuclei exhibit a clear correlation with their shell corrections δW. This is demonstrated in Fig. 3. One finds:

shell nuclei with δW < 0 are stiffer than in the LDM: $\alpha > \alpha_{LDM}$

anti-shell nuclei with δW > 0 are softer than in the LDM: $\alpha < \alpha_{LDM}$.

These specific features are the key to understand trends in the mass-dependence of fragment energies, neutron emission from fragments and structure in the mass distributions.

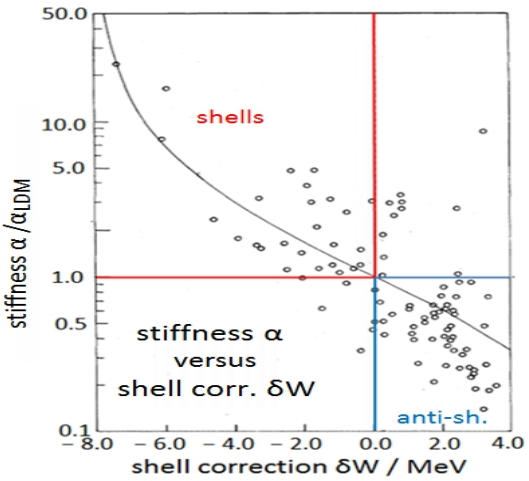

Fig. 3: Relation between relative stiffness α/α_{LDM} and shell correction δW. Adapted from [3].

The sizes of the shell and anti-shell corrections depend on the excitation energy of the nucleus. All shell corrections are fading away for increasing temperature. At temperatures T of about 2 MeV the shell effects have disappeared. A result from theory is on view in Fig. 4. It has to be stressed that with increasing excitation energy the shell nuclei become softer while anti-shell nuclei become stiffer, instead.

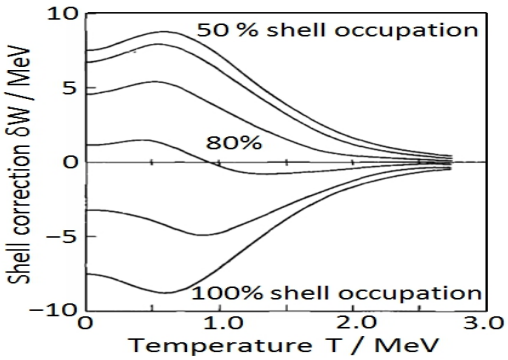

Fig. 4: Shell correction δW as a function of temperature T of the nucleus. Adapted from [4].

2 Scission Point Model

In Scission Point Models (SPM) the properties and the decay of excited fragments are discussed while the fragments are in a configuration of two separate fragments aligned on a common fission axis. The model has been explored at various levels of sophistication. The most comprehensive SPM was proposed by B. Wilkins et al. [5]. For the present discussion a rudimentary static SPM is invoked which already can give much insight into fission.

In the present model the scission configuration is visualized by two more or less deformed spheroids with the tips facing each other. Between the tips a distance d =3 to 4 fm is held constant. This is a naïve way to simulate a neck joining the two fission fragments. It is the basis of a simple SPM configuration. The potential energies V_{Coul} and V_{Def} at scission are

plotted as a function of fragment deformation in Fig. 5. The interaction energy V_{Coul} depends on the Coulomb force between deformed fragments. The total energy of deformation V_{Def} is the sum of the deformation energies for the two fragments, the deformation energy being parameterized as in eq. (3). The Q-value of the fission reaction is for a given ratio of fragment masses and charges Z_1/Z_2 independent of deformations at scission. The total energy bound as potential energy V is then

$$V = V_{Coul} + V_{Def} = Z_1Z_2 / (D_1+D_2+d) + \alpha_1(D_1 - R_{01})^2 + \alpha_2(D_2 - R_{02})^2. \quad (4)$$

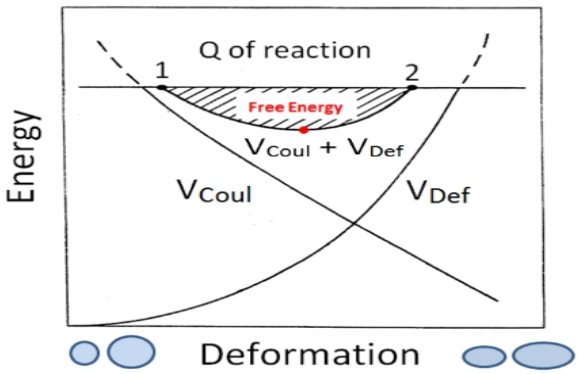

Fig. 5: Scission point model for two aligned spheroidal fission fragments, tip distance d fixed.

For increasing deformation the Coulomb repulsion V_{Coul} decreases and the deformation energy V_{Def} increases. The energy V_{Coul} forms the main part of the total kinetic energy TKE of fragments after scission, while after scission and relaxation of deformation the energy V_{Def} turns into excitation energy of fragments. It contributes to the total excitation energy TXE of fragments. The difference between the energy set free at scission Q and the energy bound as potential energy $V = V_{Coul} + V_{Def}$ is available to feed the pre-scission kinetic energy E_{Kpre} and the intrinsic excitation energy E_{int}^* the fragments already have at scission. The two energies contribute to TKE and TXE, respectively. Their sum is called "free energy" E_{free} :

$$E_{free} = E_{Kpre} + E_{int}^*. \quad (5)$$

Note that E_{free} is not the free energy of thermodynamics. As to be seen in Fig. 5 there are two extreme deformations where the free energy vanishes. These two limits are addressed as cold compact (1) and cold deformed (2) fission because in particular in both cases the fragments are not excited intrinsically. Conservation of energy then leads to the relation

$$Q = TKE + TXE = (V_{Coul} + E_{Kpre}) + (V_{Def} + E_{int}^*). \quad (6)$$

Finally, the red point in Fig. 5 locates the minimum of the potential energy V which in classical mechanics defines the static equilibrium. In fission this quasi-static equilibrium is identified with the average scission configuration. The conditions for a minimum for V are as usually

$$\frac{\partial V}{\partial D_1} = 0 \quad \text{and} \quad \frac{\partial V}{\partial D_2} = 0. \quad (7)$$

Evaluating these conditions one finds

$$V_{Def1} / V_{Def2} = \alpha_2 / \alpha_1. \quad (8)$$

This result is remarkable since it tells that, compared to its companion fragment, a fragment with large stiffness α carries a small deformation energy V and is hence weakly deformed, in contrast to the companion fragment with larger deformation energy and larger deformation.

3 Kinetic and excitation energies of fragments

Introducing the notion and the specific properties of shell and anti-shell nuclei in the frame of a scission point model allows to understand salient features of fragment kinetic and excitation energies.

For discussion the average total kinetic energy <TKE(A*)> as a function of the primary heavy mass A* is reproduced in Fig. 6 for the two reactions ^{240}Pu(sf) and ^{239}Pu(n_{th},f). For

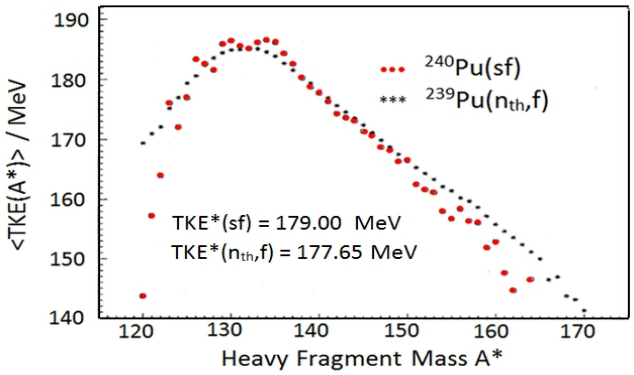

Fig. 6: Average TKE for ^{240}Pu(sf) (red) and ^{239}Pu(n_{th},f) (black) *vs* heavy primary mass A*. Adapted from [6].

both reactions the kinetic energy reaches a maximum near mass A* = 132 and decreases towards asymmetric and symmetric fission. The energy dip of symmetric compared to asymmetric fission is very pronounced for the (sf) reaction. The dip amounts to more than 40 MeV. This is by far larger than the decrease of the Q-value when going from its maximum at A*= 132 to symmetry at A* = 120 which does not exceed some 5 MeV, typical for all actinides. The main reason for the energy dip is that at symmetry two soft anti-shell fragments with A* = 120 are facing each other (see Fig.2). In the SPM of Fig. 5 the deformation potential V_{Def} hence rises very gently and the average scission configuration at the minimum of the total potential V moves to very elongated shapes of the fragments. In consequence the kinetic energy TKE will become small and create a dip. For mass asymmetry being steered by shell nuclei near A = 132 (Z = 50, N = 82) the stiff shell nucleus will shift the scission point towards compact scission shapes with large Coulomb potential and eventually large kinetic energy TKE as observed. Finally, for super-asymmetric fission with $A_{LF} \approx 80$ u and $A_{HF} \approx 160$ u the shell corrections are close to $\delta W = 0$ and $\delta W >> 0$, respectively. The scission configuration is expected to be elongated and the TKE ensues to become small. However,

for asymmetric fission the decrease of the Q-value with increasing asymmetry contributes to a large fraction, but not fully, to the decease of TKE found in experiment.

More revealing is in Fig. 6 the comparison between spontaneous and n-induced fission of ^{240}Pu. For increasing excitation, the kinetic energy increases for both symmetric and far-asymmetric fission, but surprisingly decreases for asymmetric fission. This is readily understood taking into account the fading away of shell and anti-shell effects. At higher excitation energy the shell fragments become softer and anti-shell fragments stiffer. Hence the scission configurations will be more stretched or more compact, respectively, and kinetic energies decease or increase.

The influence of shell and anti-shell effects is perhaps even more conspicuous in the excitation energies of fragments. As already indicated above, the deformation energy of fragments at scission turns into intrinsic excitation after relaxation of deformation following scission. To the total excitation energy contribute also the excitation already present at scission as outlined in eq. (6). The excitation energies are exhausted by neutron evaporation and by gamma emission once neutron evaporation has stopped. In low energy fission the deformation energy of eq. (3) is the main supply of excitation and neutrons evacuate the main part of excitation. In spite of these reservations neutron multiplicity may be considered to fairly reproduce the deformation energy at scission.

The famous sawtooth of neutron multiplicity as a function of fragment mass number is an often discussed puzzle. It is on display in Fig. 7 for the reaction ^{235}U(n$_{th}$,f). Full points are

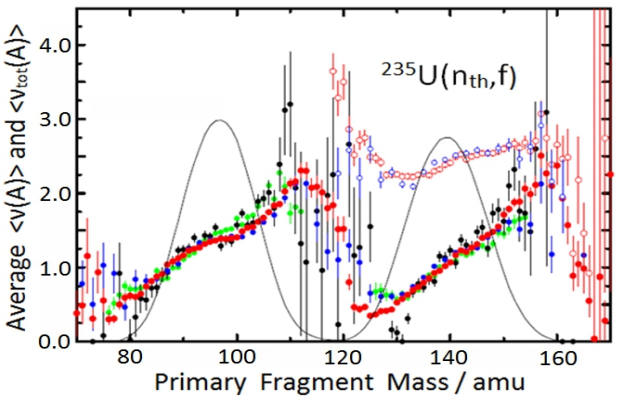

Fig. 7: Multiplicity of neutrons evaporated from fragments in ^{235}U(n$_{th}$,f). Adapted from [7].

average multiplicities <ν(A)> from different authors and open points are the average total multiplicity <ν$_{tot}$(A$_H$> from both fragments plotted depending on the heavy fragment mass. The jump in multiplicity from $A_L \approx 112$ to $A_H \approx 128$ is spectacular. A look to Fig. 2 identifies for these masses an anti-shell and a shell fragment, i.e. a soft and a stiff nucleus. The SPM predicts in eq. (8) for this combination a large deformation energy for the soft and a small deformation energy for the stiff nucleus to be reflected in the neutron multiplicities. This is what is observed in experiment.

In Fig. 7 the total neutron multiplicity <ν$_{tot}$(A$_H$)> rises for symmetric fission. This is just due to the fact that at symmetry two anti-shell nuclei with masses A = 118 are facing each other in the SPM. The scission configuration is hence stretched as already argued in connection with the kinetic energy dip at symmetry (see Fig. 6). The rise of deformation energies as manifested by neutron multiplicities compensates the kinetic energy dip at

symmetry. In other words, the total energy release is pretty constant as calculated for the Q-values from mass tables.

Finally, one may ask how the sawtooth develops when the excitation energy of the fissioning nucleus is raised. Experimental results are on view in Fig. 8. Neutron multiplicities ν(A) are shown for a wide range of excitation energies in two reactions leading to the same

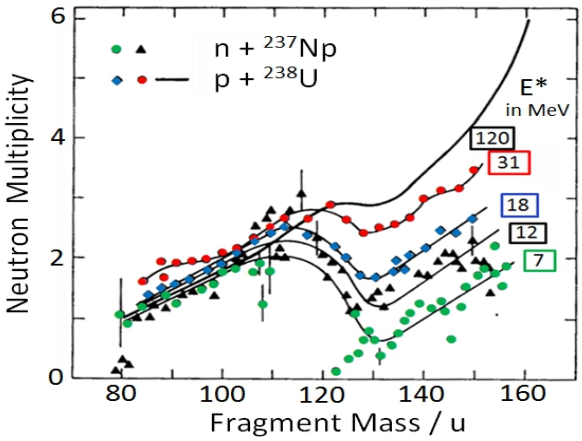

Fig. 8: Neutron multiplicities as a function of excitation energy in the two reaction ^{237}Np(n,f) and ^{238}U(p,f) forming the same compound nucleus ^{238}Np. Adapted from [8].

compound nucleus ^{238}Np. When the excitation energy of the fissioning compound is increased, the neutron multiplicity for the light fragment stays virtually constant while for the heavy fragment the neutron multiplicity increases dramatically. The interpretation in the SPM is straightforward. Shell and anti-shell corrections fade out with excitation. Soft anti-shell nuclei near A ≈ 112 become stiffer and stiff shell nuclei near A ≈ 130 become softer. Hence fragment deformations at scission are shifted from the light to the heavy fragment. At high excitation energies a smooth multiplicity curve ν(A) as predicted by the LDM results.

4 Symmetric and asymmetric fission modes

Soon after the discovery of fission it became evident that in fission of the standard actinides the mass distributions of fragment yields are asymmetric, with one lighter and one heavier fragment. This is in conflict with the LDM and it remained a puzzle until shell effects in nuclei became known. However, besides asymmetric fission there is always a symmetric component. The notion of two different fission "modes" was proposed in 1951 by Turkevich-Niday [9].

The two modes differ both in mass and energy distributions. They evolve differently as a function of excitation energy. In Fig. 9 the fragment mass distribution for the reaction ^{232}Th(n,f) is on display for several incoming neutron energies. At low excitation the symmetric yield is by orders of magnitude lower than the asymmetric one. But with increasing excitation the symmetric yield catches up rather quickly. This finding suggests that the two modes have to overcome different barriers.

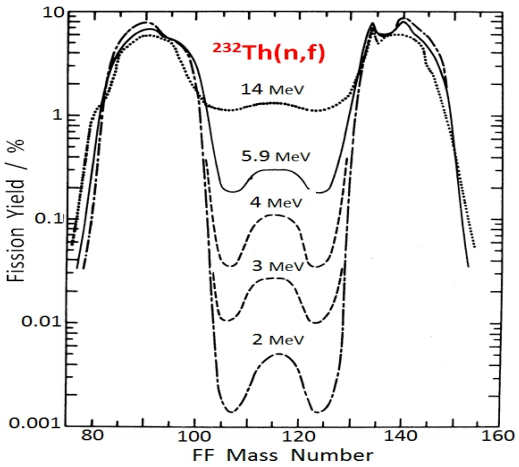

Fig. 9: Mass distribution for ^{232}Th(n,f) *vs* incoming neutron energy. Adapted from [10].

There has been much theoretical work exploring the potential energy surface (PES) of a deforming nucleus taking into account at least two deformation parameters describing the elongation and the necking in of the nucleus. In a cut through the PES along the path of minimum action leading to scission the structure of the barrier is double-humped (if not triple-humped). The structure of the barrier is sketched in Fig. 10. Starting from the ground

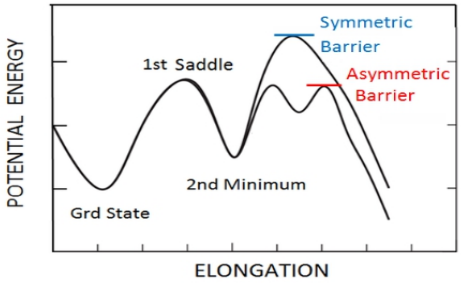

Fig. 10: Cut through the PES of deformation. Two paths lead to scission. Adapted from 11].

state towards scission a first saddle has to be overcome. At this stage the nucleus is axially asymmetric but still symmetric in mass. A second minimum in the PES is then reached. Near this minimum a bifurcation gives the nucleus the choice between two paths. A first path has a lower barrier where the shape of the nucleus is asymmetric resembling a pear. After scission this will be observed as asymmetric fragment mass division. A second path has a higher barrier to surmount but which in contrast to the first path is symmetric in mass. This is the origin of symmetric mass divisions. The structure of the PES is hence seen to be at the basis of experiments like the one in Fig. 9. Symmetric and asymmetric fission follow different paths with differing barriers in the PES.

The kinetic energy distributions of fragments bring out even more clearly that the two modes are really distinct. The energy dip near mass symmetry in the TKE was traced in the above to the anti-shell structure of the respective fragments while for asymmetric fission shell

stabilized nuclei are dominant. Elongated and compact scission configurations with low and large TKE, respectively, are resulting.

In Fig. 11 TKE distributions are visualized for a few masses A_H near mass symmetry for the reaction ^{234}U(n,f). The incoming neutron energy is 4.91 MeV. At symmetry the TKE

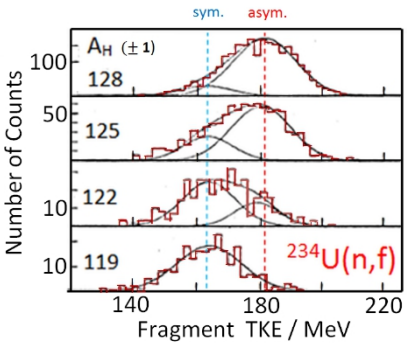

Fig. 11: TKE distributions near symmetry for the reaction ^{234}U(n,f). Adapted from [12].

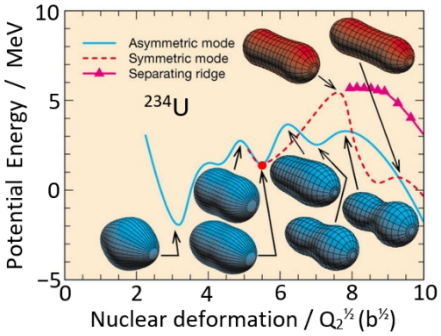

Fig. 12: PES near the barriers for ^{234}U. Adapted from [11].

distribution is well represented by a Gaussian. Also for masses in the asymmetric wing the TKE distributions are again Gaussians but pushed to larger energies by almost 20 MeV. For masses in the transition region from symmetric to asymmetric fission, however, the distributions are skewed and broad. The skewed distributions are fitted by two Gaussians shifted by the almost 20 MeV from above. The Gaussians represent symmetric and asymmetric contributions in the overlap region of the two modes, fading away or surging when moving away from symmetric to asymmetric mass distributions, respectively. The fit is perfect. It proves that the modes are and remain distinct with no mixing, just simply overlapping two shifted distributions with varying weight.

Modern calculations of the PES of ^{234}U corroborate the experimental findings. This is shown in Fig. 12. As a function of deformation one distinguishes two paths with different barriers to scission. As in Fig. 10 there is the double humped asymmetric barrier (blue line) and a higher symmetric barrier (pointed red). The respective shapes of the nuclei are visualized. But what was not shown in Fig. 10 is a high ridge separating the two modes (red triangles). The ridge prevents any spilling over from one mode to the other. This is precisely as observed in Fig. 11.

Besides the manifestly distinct modes, symmetric and asymmetric, known since 1951 it was realized much later that the asymmetric mode exhibits a fine structure. The asymmetric mode is itself bimodal. These two fine structure modes are subtler to identify and characterize. They were probably first recognized in the mass and TKE distributions of fragments in the actinides. At closer look these distributions are not plain Gaussians. Instead they are a superposition of two slightly shifted Gaussians. An example is provided in the Figs. 13 and 14. For the reaction ^{240}Pu(sf) both the fragment mass and TKE distributions

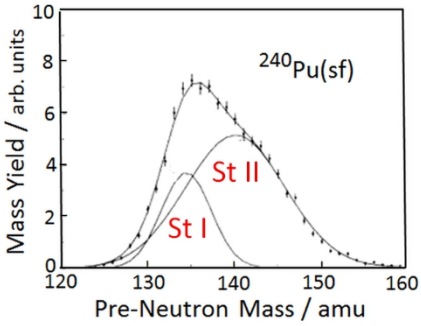

Fig- 13: Mass distribution for ^{240}Pu(sf). Adapted from [13].

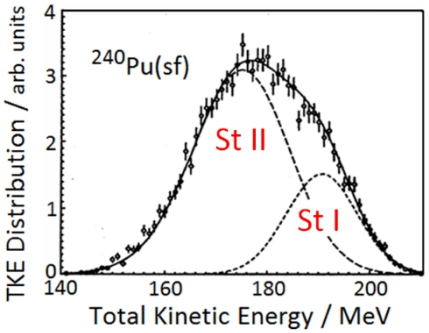

FIG. 14: TKE distribution for ^{240}Pu(sf). Adapted from [14].

exhibit a distorted non-Gaussian shape. But the distributions are well reproduced by a superposition of two Gaussians which are interpreted as two different asymmetric modes. The modes were studied in countless experiments. A theoretical basis was developed by U. Brosa, S. Grossmann and A Müller [15]. In scrutinizing the PES from the barrier down to scission a multitude of paths were discovered. Besides a superlong (SL) path for symmetric fission, the most prominent ones are two paths for asymmetric fission which were called Standard I (St I) and Standard II (St II). Each of these modes have characteristic mass and energy distributions. An analysis of the mass distribution for ^{235}U(n,f) in terms of Gaussian shaped modes is given in Fig. 15. The St I mode has the average mass A_{StI} = 132 u and the

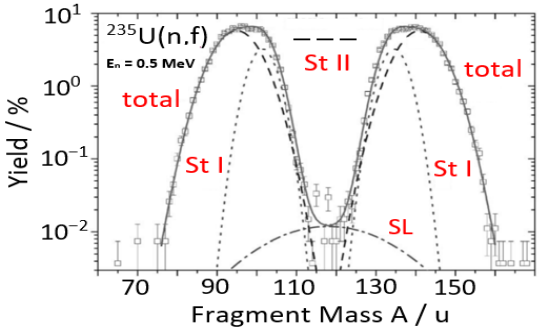

Fig. 15: Mode decomposition of the mass distribution for ^{235}U(n,f) at the incoming neutron energy E_n = 0.5 MeV. Adapted from [16].

mode St II has on average A_{StII} = 142 u. The kinetic energy TKE at these masses are also very different. For St I it is $TKE_{St\ I}$ = 187 MeV and for St II it is $TKE_{St\ II}$ = 167 MeV.

The physics behind the two standard asymmetric modes St I and St II is discussed in terms of shell effects, once for spherical and once for deformed fragments. Long before standard asymmetric modes came into view, B. Wilkins et al. explored already in 1976 a scission point model where deformed shells played a major role. In particular, the neutron number N of heavier nuclei was pivotal. For N = 82 there is a pronounced shell effect for a spherical shape of the nucleus which is well known since long. However, at elongated deformations there appears again a strong shell effect for N = 88. These neutron numbers are characteristic for the modes St I and St II, respectively. Except for very heavy actinides where mass

distributions become symmetric, throughout the actinides the heavy group of asymmetric fission is fixed by (A_H = 132, N_H = 82, Z_H = 50) for St I and (A_H = 142, N_H = 88, Z_H = 54) for St II. The change in mass number of the compound nucleus when sweeping through the actinides is only followed by the light fragment group. It is further noteworthy that the kinetic energies TKE for the St I mode are always larger than for the mode St II. This is in accordance with the spherical and elongated structure of the key nuclei involved, respectively. However, relative yields of modes St I and St II can vary abruptly from one actinide to the next.

It is generally accepted that as outlined in the above the fine structure St I and St II of asymmetric fission is closely linked to fragment shell properties. In all variants of PES calculations no indications of fragment properties are reported right at the saddle point. However, once the saddle point has been passed, properties of fragments start to be noticed. Yet, no PES calculations are known locating precisely where on the way to scission a bifurcation into St I and St II becomes manifest. Anyhow, in the discussion of some experiments it is still claimed that like the symmetric-asymmetric bifurcation also the fine structure bifurcation is due to different saddle points for St I and St II. It is therefore worthwhile to inspect a series of experiments on angular distributions of fragments which could give a clue on the issue.

5 Angular distributions of fission fragments

In the early phase of fission research the angular distributions of fission fragments have been extensively studied. A focus was placed on neutron induced fission of e-e target nuclei for neutron energies near the fission barrier. In the following the reaction ^{234}U(n,f) is inspected.

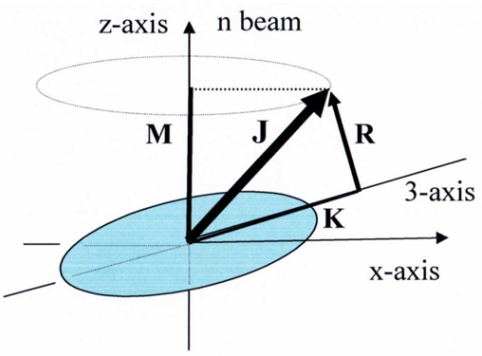

Fig. 16: Angular momenta of a deformed nucleus with **J** = total momentum and its components M, K and R. The 3-axis is the fission axis.

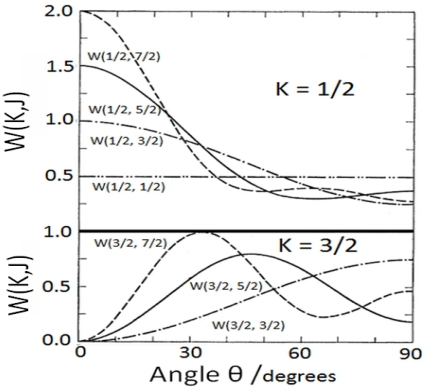

Fig. 17: Angular distributions of fragments for (n,f) reactions with e-e target (spin I = 0). Adapted from [17]

In Fig. 16 the angular momentum **J** and its components are presented. M and K are the projections of **J** on a space-fixed axis (n beam) and the axis of deformation (3 axis). R is the angular momentum perpendicular to the deformation axis observed as fission axis in experiment. The good quantum numbers are J, M and K. Fragment emission angles Θ are measured relative to the direction of the neutron beam inducing fission. From the quantum mechanics of a symmetric top the angular distribution W^J_{MK} (Θ) of fragments is found as the orientation of the deformation axis:

$$W^{J}_{MK}(\Theta) \sim | D^{J}_{MK} |^{2} \quad (9)$$

with D^{J}_{MK} the wavefunction of a symmetric top. The corresponding angular distributions of the fragments are displayed in Fig.17. The labels on the curves are W(K,J). Only K-values 1/2 and 3/2 are considered since higher K-values come only at higher excitation energies into play. Notably the character of the distributions depends essentially on the K-numbers. For K-numbers K = ½ fragments are emitted along the beam axis ($\Theta = 0°$) and for K = 3/2 sideways ($\Theta > 0°$). It should be underlined that mainly the K quantum numbers characterize the angular distributions. They hence provide rather detailed information on the angular momenta in fission.

In the following fragment angular distributions from fission of ^{234}U(n,f) are compared for incoming neutrons above and below the fission barrier. From the plot in Fig. 18 the barriers

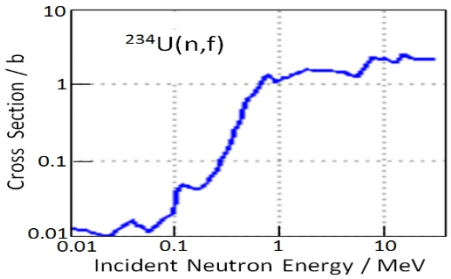

Fig. 18: Fission cross section σ(n,f) for the reaction ^{234}U(n,f) from thermal to MeV neutrons.

are read to be B_f = 1.2 MeV for first chance fission and B_f = 5.3 MeV for second chance fission. There is a major difference between above-barrier and sub-barrier fission. Only for above-barrier fission the nucleus will pass over a saddle point with a well-defined transition state with quantum numbers J and K. For sub-barrier fission there is no such transition state. In presence of a transition state above the barrier A. Bohr postulated that the quantum numbers (K,J) of this state will be preserved down to scission. They determine the angular distributions of fragments. Since for the Turkevich-Niday modes the barriers and hence the transition states differ for symmetric and asymmetric fission, the angular distributions of the two modes will not be identical. For the Brosa modes, by contrast, it was argued above that they are not yet differentiated at the barrier. On condition the argument is valid, the modes St I and St II share the same transition state and according to A. Bohr carry the same quantum numbers (J,K). The angular distributions will then be identical for the two modes. The distributions will hence neither depend on fragment mass nor fragment kinetic energy. This should be true whatever the ratio of yields St I and St II may be. Evidently, when varying the excitation energy of the fissioning compound, the angular distributions could in general change.

For the reaction ^{234}U(n,f) under study the anisotropy W(0°) / W(90°) of the angular distribution is plotted in Fig. 19 averaged over the neutron energy range $1.2 < E_n < 3.5$ MeV as a function of the heavy fragment mass. The anisotropy stays indeed constant over the full range of asymmetric fission. It corroborates the statement that the modes St I and St II evolve from the same transition state at the saddle which according to A. Bohr impose the same (J,K) assignments on the two modes.

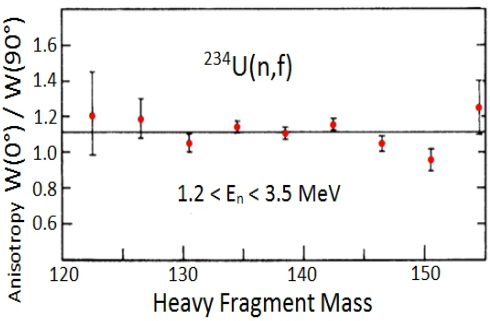

Fig. 19: Anisotropy of fragment angular distribution from ^{234}U(n,f) averaged over the neutron energy 1.2 < E_n < 3.5 MeV. Adapted from [19].

Resonances in the sub-barrier fission cross section have raised interest since long. They were not expected in the LDM model. Only when the double–humped structure of the fission barrier became known, calculations of the transmission showed resonances when β-vibrations in the second minimum are excited. The investigation of fragment angular distributions near resonances in the sub-barrier fission cross section has disclosed surprising features not observed in above-barrier fission.

Experimentally the low cross sections have not encouraged many workers to enter the field. Most research was done for (n,f) reactions with e-e targets like ^{234}U. Results from a recent comprehensive study for ^{234}U(n,f) are on display in Fig. 20. The fission cross section σ(n,f) is given for incoming neutron energies up to E_n = 2.0 MeV (black line). Below the fission barrier at E_n = 1.2 MeV two resonances at E_n = 0.55 and E_n = 0.77 MeV come into view (note that in the logarithmic plot of Fig. 18 still more resonances at lower energy E_n are observed). Experimental mass and TKE distributions were investigated at two angles Θ of

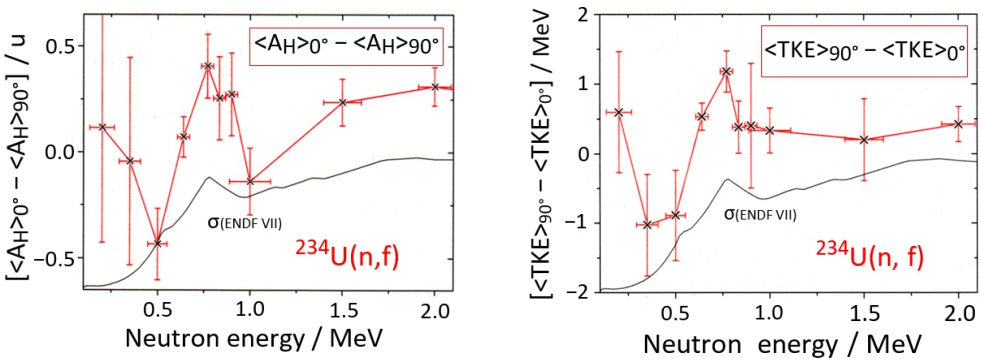

Fig. 20: Besides the fission cross section σ the differences for the average heavy mass <A_H> and the average kinetic energy <TKE> at two fragment angles Θ = 0° and Θ = 90° are shown for neutron energies up to 2.0 MeV. Adapted from [20].

fragment emission relative to the neutron beam: Θ = 0° and Θ = 90°. To characterize the distributions, the average heavy fragment mass <A_H> and the average kinetic energy <TKE> were determined for the two angles Θ. For the final results in Fig. 20 the difference at the two angles was evaluated as a function of neutron energy. At the two resonances in cross section these differences are strongly fluctuating with excursions to positive and negative

values. Consider e.g. the resonance at E_n = 0.77 MeV. Evidently the average mass $<A_H>$ at Θ = 0° is larger than at 90°. Simultaneously the average <TKE> is smaller at Θ = 0° than at 90° (note that in the figure for the differences of mass and energy the sequence of angles is interchanged). With reference to Figs. 13 and 14 this is equivalent to the statement that upon comparing the two angles, the Brosa mode St II is boosted at angle Θ = 0°. In view of Fig. 17 it tells that the yield for quantum number K = 3/2 is reinforced in the mode St II compared to mode St I.

A similar reasoning is applied in the analysis of mass and energy distributions for the resonance at lower neutron energy E_n = 0.55 MeV. Here the average mass $<A_H>$ rises and the average energy <TKE> drops at the angle Θ = 90°. With reference to Fig. 17 the yield for the quantum number K = 1/ 2 is raised for the mode St II compared to mode St I.

In both resonances below the barrier the fragment angular distributions are mode dependent. The modes St I and St II carry different sets of (J, K). As to the A. Bohr postulate, it is manifestly valid for fission passing over the barrier. There the same angular momenta (J,K) defined by the transitions state are imposed on both modes. This just tells that the total angular momentum J and its projection K on the fission axis stay constant from saddle to scission. But the postulate loses its validity in sub-barrier resonances.

One may speculate why only transition states at the saddle point impart their angular momenta (J,K) to both subsequent Brosa modes. In sub-barrier fission, β-vibrational states in the second minimum of the PES are fostering tunnelling. This is the cause for resonances. One may then wonder whether the quantum numbers of the vibrations could not play a similar role like the transition states. The difference is that in above-barrier fission the quantum numbers of the transition state are settled with no mode valleys yet in view, while in sub-barrier fission the nucleus emerges in the PES landscape between saddle and scission where the valleys of the Brosa modes have already taken shape. Resonant tunnelling there efficiently assists the standard tunnelling process. The two mechanisms will have their own sets of (J,K) quantum numbers and each mechanism will confer its (J,K) assignment to the modes with varying specific weights. In the sum the set of (J,K) values will then be different for the two modes giving rise to the fragment mass and kinetic energy dependence of the angular distribution W(Θ).

6 Conclusion

The present survey proposes to trace the interplay between shell structure of fission fragments and fission modes. Since when talking about shell effects the stabilizing of nuclei is usually understood, it is first pointed out that shell structure is as often stabilizing as de-stabilizing the Liquid Drop. The terms shells and anti-shells are introduced to help memorize the difference for shell corrections being either negative or positive, respectively. A fundamental property of shells and anti-shells is their stiffness against deformation which is larger or smaller than in the LDM, respectively. The energetics of the fission process is discussed in a scission point model which even in a rudimentary version allows to understand many fission phenomena. Out of a huge body of pertinent data a sample of a few experiment is selected where shell and anti-shell effects are catching the eye.

Fission modes were first introduced phenomenologically by Turkevich-Niday in 1951. The purpose was to describe the different properties of symmetric and asymmetric fission. The difference is nowadays understood to be due to different paths of the fissioning nucleus being available in deformation space. The detailed analysis of the potential energy surface for a nucleus on its way to scission describes the fission barrier to be double-humped. In the second minimum of the barrier a bifurcation points opens the way to symmetric fission with

a barrier somewhat higher than for asymmetric fission. The complex structure of the barrier is displayed in Fig. 21. The two modes employ two transition states with different (J,K)

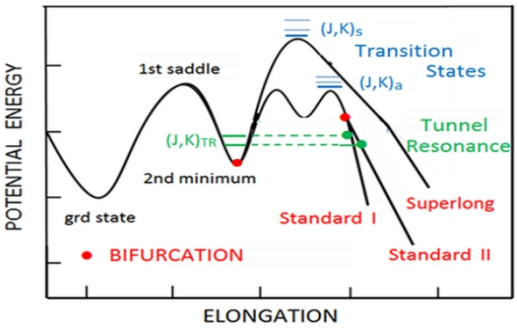

Fig. 21: PES near the barrier with bifurcation points for Turkevich-Niday and Brosa modes.

assignments. Since the quantum numbers (J,K) determine the angular distribution W(Θ) of fragment emission, the angular distributions for symmetric and asymmetric fission are different. Remarkably the fragments from symmetric fission are anti-shell nuclei while for asymmetric fission shell nuclei are dominant.

The fragment mass and energy distributions in asymmetric fission exhibit a fine structure. According to U. Brosa et al. two modes, Standard I and Standard II, contribute. Very closely the modes are linked to the neutron numbers N = 82 and N = 88 in the heavy fragment group. For both neutron numbers there is a strong shell effect, but once for a spherical and once for a deformed shape of fragments at scission. At the saddle point these fragment properties are not yet in view. Therefore the bifurcation for the Brosa modes must lie somewhere between saddle and scission as indicated in Fig. 21. However, both modes adopt the same angular momentum (J,K) signatures of the transition state at saddle. This rule was postulated by A. Bohr. In consequence the angular distributions are identical for the two modes. There is no dependence on fragment mass and/or energy. Yet, for sub-barrier fission a different situation obtains. In particular, in tunnel resonances the angular distributions are mode-dependent. Tunnel resonances are enhanced by β-vibrations in the second minimum of the potential energy surface and it is tempting to expect the (J,K) assignments of the vibrations taking over the role of the transition states in above-barrier fission. This however is not the case. Two mechanisms of tunnelling have to be taken into account: standard tunnelling bolstered by resonant tunnelling. The two mechanisms will confer different sets of quantum numbers (J,K) to the modes with different overall weight. In the sum the set of (J,K) contributions to the modes will not be the same and the angular distributions become mode dependent. As visualized schematically in Fig. 21, in resonances the Brosa modes are fed differently. This is directly evident from the mass and energy dependence of angular distributions.

The story of shells, anti-shells and modes is not limited to fission of actinides. The issues addressed here have been studied by M. Itkis et al. for the pre-actinides down to compound mass numbers of $A_{CN} = 200$ [21]. For heavy actinides and beyond E.K. Hulet has discovered bimodal symmetric fission [22]. In heavy ion induced fission new fission phenomena like quasi-fission show up. These topics are not reviewed in the present survey.

References

1. W.D. Myers and W.J. Swiatecki, Nucl. Phys. **81**, 1 (1966)
2. A. Ruben, H, Märten, D. Seeliger, Z. Phys. A **338**, 67 (1991)
3. M. Kildir, N.K. Aras, Phys. Rev. C **25**, 365 (1982)
4. A.S. Jensen, J. Damgaard, Nucl. Phys. A **203**, 578 (1973)
5. B.D. Wilkins, E.P. Steinberg, R.R. Chasman, Phys. Rev. C **14**, 1832 (1976)
6. C. Wagemans et al., Phys. Rev. C **30**, 218 (1984)
7. A.S. Vorobyev et al., *Interactions of Neutrons with Nuclei* **17**, 60 (2009)
8. D. Hilscher, H. Rossner, Ann. Phys. France **17**, 471 (1992)
9. A. Turkevich, J.B. Niday, Phys. Rev. **84**, 52 (1951)
10. L.E. Glendenin et al., Phys. Rev. C **22**, 152 (1980)
11. P. Möller, Nature **409**, 788 (2001)
12. W. Holubarsch, PhD thesis, Univ. of Tübingen, Germany (1971)
13. C. Wagemans, P. Schillebeeckx, Nucl. Phys. A **502**, 287c (1989)
14. L. Dematté et al., Nucl. Phys. A **617**, 331 (1997)
15. U. Brosa, S. Grossmann, A. Müller, Phys. Rep. **197**, 167 (1990)
16. F.-J. Hambsch et al., *Seminar on Fission* **V**, 47 (2003)
17. A. N. Behkami et al., Nucl. Phys. A **118**, 65 (1968)
18. A. Bohr, *Peaceful Uses of Atomic Energy* **2,** 151 (1955)
19. R. Vandenbosch, J.P. Unik, J.R. Huizenga, *Phys. and Chem. of Fission* **1**, 547 (1965)
20. A. Al-Adili, PhD thesis, Uppsala University, Sweden (2013)
21. M. Itkis et al., Sov. J. Nucl. Phys. **53**, 764 (1991)
22. E.K. Hulet, Phys. At. Nucl. **57**, 1099 (1994)